Performance maps for the control of thermal energy storage

Christian Finck[1][*], Rongling Li[2], Wim Zeiler[1]
[1] Eindhoven University of Technology, Eindhoven, the Netherlands
[2] Technical University of Denmark, Denmark
[*] email: c.j.finck@tue.nl

Abstract

Predictive control in building energy systems requires the integration of the building, building system, and component dynamics. The prediction accuracy of these dynamics is crucial for practical applications. This paper introduces performance maps for the control of water tanks, phase change material tanks, and thermochemical material tanks. The results show that these performance maps can fully account for the dynamics of thermal energy storage tanks.

Introduction

The potential of thermal energy storage (TES) as a source of demand side flexibility is becoming a popular research topic. Several researchers emphasize the importance of the interaction between TES, thermal and electrical appliances to fully describe the flexibility of building energy systems (De Coninck and Helsen, 2016; Oldewurtel et al., 2013; Ottesen and Tomasgard, 2015). To quantify this flexibility, capturing the dynamic behavior of the system and components is a prerequisite (Masy et al., 2015; Patteeuw et al., 2015). This is because dynamic behaviors play a major role in the scheduling of TES in predictive control. However, current control methods for TES tanks, such as water tanks and ice tanks, only use simple TES models such as low order resistance-capacitance (RC) network models.

This study aims to provide a methodology for the integration of the storage dynamics into predictive control. For this purpose, performance maps of TES are developed to describe the dynamics of TES.

Methodology

Matlab is used as a platform to simulate the dynamic behavior of TES, including the main heat and mass transfer effects, initial conditions that can be the actual state of charge, and the boundary conditions. During charging, discharging and rest mode, the ability of the storage tank to respond to changes in boundary conditions is simulated, which includes charging, discharging temperature and velocity of the heat transfer medium. The resulting changes in the state of charge; charging, discharging power; and charging, discharging temperatures are presented in performance maps. A water tank without an internal heat exchanger, a phase change material (PCM) tank and a thermochemical material (TCM) tank including internal heat exchanger are simulated. The TES tank models are based on the one-dimensional convection-diffusion-reaction equation. Previous case studies have shown that a one-dimensional approach can represent the behavior of water tanks (Appadu and Appadu, 2013; Karahan, 2006; Shukla et al., 2011), PCM tanks (Hu and Argyropoulos, 1996; Lo Brano et al., 2014), and TCM tanks (Finck, C.J. et al.; Pesaran et al., 2016). We use the Crank-Nicolson scheme, a finite difference method, to numerically solve the one-dimensional convection-diffusion-reaction equation.

Design of thermal energy storage tanks

A stratified water tank, a packed bed reactor with PCM and a packed bed reactor with TCM are designed. The TES tanks are cylindrical vessels with a volume of 0.5 m³. For all TES tanks, the volume flow of the external heat transfer media is 1 m³/h.

It is to emphasize that all TES tanks are equipped with standard insulation material of 0.032 m thickness and 0.033 W/mK of thermal conductivity to reduce thermal losses to the environment.

The water tank has two flow connections, one at the top and another one at the bottom for supply and return water. To establish thermal stratification during charging, hot water enters the top and colder water leaves at the bottom. For discharging, inflow and outflow are opposite.

The PCM tank consists of a heat exchanger in which water as heat transfer fluid passes through a copper coil. A PCM layer of 0.02 m is applied to the surface of the copper tubes. The heat transfer area between the copper coil and the PCM is 8 m². Two different materials are chosen as PCM, $CaCl_2 \cdot 6H_2O$ and lauric acid (Table 1). The mass of lauric acid (307 kg) and $CaCl_2 \cdot 6H_2O$ (521 kg) are calculated.

The TCM tank consists of a sorption unit and an evaporator/condenser unit. The evaporator/condenser is assumed to be a constant low-temperature source. Explicit design for the evaporator/condenser unit is not considered in this study. The TCM sorption unit has a heat exchanger as similar to the PCM tank. Heat is exchanged through a copper coil between water flow and

TCM layer with a heat transfer area of 8 m². A layer of 0.02 m is applied to the copper tubes. The TCMs considered in this case study are zeolite13X-water and silica gel-water (Table 2).

Table 1: Properties of PCM ($CaCl_2 \cdot 6H_2O$) (Mosaffa et al., 2014) and (Lauric acid) (Pereira da Cunha and Eames, 2016)

Parameters		$CaCl_2 \cdot 6H_2O$	Lauric acid
Melting point [°C]		29	44
Melting enthalpy [kJ/kg]		191	212
Density [kg/m³]	Solid	1710	1007
	Liquid	1530	870
Specific heat [J/kgK]	Solid	2200	2020
	Liquid	1400	2150
Thermal conductivity [W/mK]	Solid	1.09	0.22
	Liquid	0.54	0.15

Table 2: Properties of TCM (zeolite13X-water) (Leong and Liu, 2006; Sayılgan et al., 2016) and (silica gel-water) (Deshmukh et al.; Lim et al., 2017)

Parameters	zeolite13X-water	Silica gel-water
Adsorption enthalpy [kJ/kg]	3.2e03	2.8e03
Density [kg/m³]	620	730
Specific heat [J/kgK]	836	924
Thermal conductivity [W/mK]	0.2	0.17
Diffusion coefficient [m²/s]	7.5e-09	7.5e-09

The usage of zeolite-water and silica gel-water as thermochemical heat storage materials can be found in many previous studies (Deshmukh et al.; Finck et al., 2014; Hauer, 2007; Tatsidjodoung et al., 2016). The hydrothermal, mechanical stability and the favorable corrosion behavior make these TCMs suitable as candidates for experimental investigations. The mass of zeolite13X-water (189 kg) and silica gel-water (222 kg) are calculated.

Modelling framework

A one-dimensional convection-diffusion problem including reaction term is considered to simulate the TES tanks. The convection-diffusion problem is solved numerically using the Crank-Nicolson scheme as finite-difference method. Crank-Nicolson is more accurate than other finite-difference schemes when it comes to the temporal truncation error of $O(\Delta t^2)$ (Recktenwald, 2000). The approximation using Crank-Nicolson can be written as equation (1),

$$\frac{\theta_i^{n+1} - \theta_i^n}{\Delta t} =$$

$$\frac{\alpha}{2}\left(\frac{\theta_{i+1}^{n+1} - 2\theta_i^{n+1} + \theta_{i-1}^{n+1}}{\Delta x^2} + \frac{\theta_{i+1}^n - 2\theta_i^n + \theta_{i-1}^n}{\Delta x^2}\right)$$

$$-\frac{u}{4}\left(\frac{\theta_{i+1}^{n+1} - \theta_{i-1}^{n+1} + \theta_{i+1}^n - \theta_{i-1}^n}{\Delta x}\right) + f(\theta_i^n) \quad (1)$$

in which $\theta = \theta(x, t)$ is the general variable that depends on the spatial coordinate x and the time t, α is a positive constant coefficient for the conductive term, u is a positive constant velocity for the convective term and $f(\theta_i^n)$ is the reaction term. For the simulations, the time step is one second.

This approach is applied to the water tank, PCM tank and TCM tank to simulate the main heat and mass transfer effects.

Water tank model

We assume that the stratified water tank has a vertical temperature distribution $\partial T/\partial x$. Convection and diffusion are simulated and implemented as equation (2) and (3).

$$\frac{T_i^{n+1} - T_i^n}{\Delta t} =$$

$$\frac{\alpha}{2}\left(\frac{T_{i+1}^{n+1} - 2T_i^{n+1} + T_{i-1}^{n+1}}{\Delta x^2} + \frac{T_{i+1}^n - 2T_i^n + T_{i-1}^n}{\Delta x^2}\right)$$

$$-\frac{u}{4}\left(\frac{T_{i+1}^{n+1} - T_{i-1}^{n+1} + T_{i+1}^n - T_{i-1}^n}{\Delta x}\right) \quad (2)$$

with

$$\alpha = \frac{\lambda}{\rho c_p} \quad (3)$$

where λ is the thermal conductivity, ρ is the density and c_p is the specific heat capacity of water.

PCM tank model

The PCM tank consists of a packed bed PCM reactor. The main heat transfer effects are the heat exchange between the water flow and the PCM, and the heat conduction through the PCM layer. Heat conduction during charging results in the melting process of the PCM. During discharging, solidification of the PCM takes place. To simulate the phase change, the model integrates the enthalpy change of the PCM layer as equation (4).

$$\rho\frac{\partial h}{\partial t} = \lambda\frac{\partial^2 T}{\partial x^2} \quad (4)$$

The phase change is assumed to be a non-isothermal transition between solid and liquid PCM. We use a transition phase of 2 K for the solid-liquid interface as introduced by (Lamberg, 2003). Between solidification temperature (T_{sol}) and melting temperature (T_{liq}) the thermal properties of the PCM gradually change

according to equation (5) (Hu and Argyropoulos, 1996; Lamberg, 2003).

$$h = \begin{cases} c_{p,sol}T & T < T_{sol} \\ c_{p,sol}T_{sol} + \dfrac{h_{\Delta liq,sol}(T - T_{sol})}{(T_{liq} - T_{sol})} & T < T \le T_{liq} \\ c_{p,sol}T_{sol} + h_{\Delta liq,sol} + c_{p,liq}T & T > T_{liq} \end{cases} \quad (5)$$

The heat conduction though the PCM can thus be calculated using equation (6) and (7).

$$\frac{h_i^{n+1} - h_i^n}{\Delta t} =$$

$$\frac{\alpha}{2}\left(\frac{h_{i+1}^{n+1} - 2h_i^{n+1} + h_{i-1}^{n+1}}{\Delta x^2} + \frac{h_{i+1}^n - 2h_i^n + h_{i-1}^n}{\Delta x^2}\right) \quad (6)$$

with

$$\alpha = \frac{\lambda(T)}{\rho(T)\,c_p(T)} \quad (7)$$

It is to emphasize that the PCM is homogeneous and isotropic and no natural heat convection during the melting process is considered.

TCM tank model

We assume a packed bed TCM reactor in which heat is exchanged between the external water flow and the TCM layer. During the charging process, hot water enters the heat exchanger of the sorption unit and forces the zeolite bed to desorb the attached water. The water vapor is collected in the condenser unit. During discharging, the condenser operates as an evaporator. In this case study, evaporator and condenser are modeled as a constant low-temperature source of 10 °C. The evaporator serves as water vapor source for the adsorption process. The diffusion process of the water vapor from the evaporator to the zeolite bed is simulated using the linear driving force (LDF) method as shown in equation (8).

$$\frac{d\bar{q}}{dt} = k_m\big(q_{eq} - \bar{q}\big) \quad (8)$$

In this method, the difference between equilibrium and amount of adsorbate and a constant mass transfer coefficient k_m are assumed (Pesaran et al., 2016; Rindt and Gaastra-Nedea, 2015). In the model, the values for equilibrium and amount of adsorbate are derived from the vapor pressure values that can be presented by the Clausius-Clapeyron equation (de Jong et al., 2014) as shown in equation (9)

$$\frac{dp}{dT} = \frac{\Delta h_v}{T\Delta v} \cong \frac{p\,\Delta h_v}{RT^2} \quad (9)$$

with Δh_v as molar enthalpy difference and Δv as molar volume difference of water vapor. The vapor pressure values for zeolite13X-water and silica gel-water are based on the experimental data from (Wang and LeVan,

2009). The Toth equation as shown in equation (10) is implemented as heuristic fit to the experimental data.

$$n = \frac{ap}{[1 + (bp)^t]^{1/t}} \quad (10)$$

where n is the water loading (adsorption equilibrium), p is the vapor pressure, b is an equilibrium constant, a is a constant related to the saturation capacity and t is the heterogeneity of the adsorbent (de Jong et al., 2014).

The amount of adsorbate in the zeolite bed determines the water vapor diffusion through the TCM layer that is modeled as equation (11) in which D is the effective diffusion and m_{sorb} is the mass of the dry adsorbent.

$$\frac{m_{ads,i}^{n+1} - m_{ads,i}^n}{\Delta t} =$$

$$\frac{D}{2}\left(\frac{m_{ads,i+1}^{n+1} - 2m_{ads,i}^{n+1} + m_{ads,i-1}^{n+1}}{\Delta x^2}\right.$$

$$\left. + \frac{m_{ads,i+1}^n - 2m_{ads,i}^n + m_{ads,i-1}^n}{\Delta x^2}\right)$$

$$+ m_{sorb}\left(\frac{q_i^{n+1} - q_i^n}{\Delta t}\right) \quad (11)$$

As a result from the diffusion of water vapor, the adsorption process, and the heat conduction are formulated as can be seen in equation (12).

$$\frac{T_i^{n+1} - T_i^n}{\Delta t} =$$

$$\frac{\alpha}{2}\left(\frac{T_{i+1}^{n+1} - 2T_i^{n+1} + T_{i-1}^{n+1}}{\Delta x^2} + \frac{T_{i+1}^n - 2T_i^n + T_{i-1}^n}{\Delta x^2}\right)$$

$$+ \frac{Q_s}{c_p}\left(\frac{q_i^{n+1} - q_i^n}{\Delta t}\right) \quad (12)$$

where Q_s is the adsorption enthalpy.

Performance maps of thermal energy storage

In the performance maps, all the critical information to describe the dynamic behavior of thermal energy storage tanks are considered. Performance maps of TES tanks can show the heat and mass transfer dynamics for any operation during charging, discharging or idle mode. Therefore, any disturbance applied to a TES tank is implemented in a performance map. These disturbances are operational parameters such as the temperature and velocity of the external water flow (heat transfer medium) and the environmental conditions where the TES tank is placed. Based on the disturbances and the actual state of charge, the performance of the TES tank can be simulated for a certain control time step. Based on the TES tank models as introduced in the previous sections, the individual performance maps are simulated for the charging case. Two different constant charging temperatures are used to compare the response of the TES tanks. For the water tank and PCM tank, constant charging temperatures of 60 °C and 95 °C are chosen.

BUILDING
SIMULATION 2017

INTERNATIONAL
BUILDING
PERFORMANCE
SIMULATION
ASSOCIATION

For the TCM tank, 95 °C and 120 °C of constant charging temperatures are used because desorption occurs at higher temperatures.

It is to emphasize that the following performance maps are illustrated using a normalized energy capacity (0 % to 100 %).

Results

Performance maps of water thermal energy storage

Figure 1 shows the performance maps of the stratified water tank charged from 21 °C. As can be seen, the water tank quickly responds to the charging temperature. In the charging phase from 0 % to 70 %, hot water with 95 °C or 60 °C enters the top and leaves the bottom with 21 °C. During this phase, thermal stratification is established and the resulting charging power is constant. While charging the water tank from 70 % to 100 %, hot water displaces colder water at the bottom. The water outlet temperature increases and the temperature difference between inlet and outlet decreases. During this phase, the charging power drops to the point that the water tank is fully charged. The entire charging process is finished after 44 min.
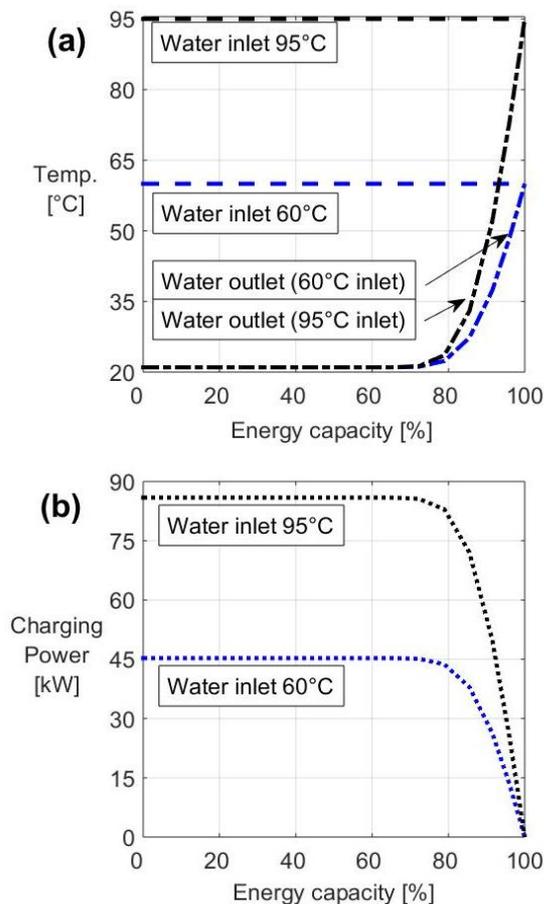

Figure 1: Water tank performance maps for charging from 0 % (21 °C) to 100 % (60 °C and 95 °C); (a) inlet and outlet water temperatures over energy capacity; (b) charging power over energy capacity.

Performance maps of PCM thermal energy storage

Figure 2 shows the performance maps of the PCM tank using $CaCl_2 \cdot 6H_2O$ as PCM. The simulation for this specific charging case starts at a PCM temperature of 21 °C in which the PCM is in a solid state. Hot water of 95 °C or 60 °C enters the heat exchanger and heats up the PCM quickly until the melting point of 29 °C is reached. While melting occurs the charging power gradually decreases, as can be seen for 95 °C charging between 0 % and 60 % and for 60 °C charging between 0 % and 70 %. The reason for the decrease of the charging power during the melting process is the change of the thermal properties of the PCM such as specific heat capacity, density, and thermal conductivity that are temperature dependent. After 60 % of energy capacity at 95 °C charging and after 70 % of energy capacity at 60 °C charging the PCM is molten. Further charging results in a temperature increase of the whole PCM layer, so that only sensible heat is stored in the PCM. The temperature increase of the PCM results in a smaller temperature difference between water inlet and outlet and a decrease of charging power to the point where the PCM temperature is identical to the water inlet temperature. The entire charging process is finished after 8 h.
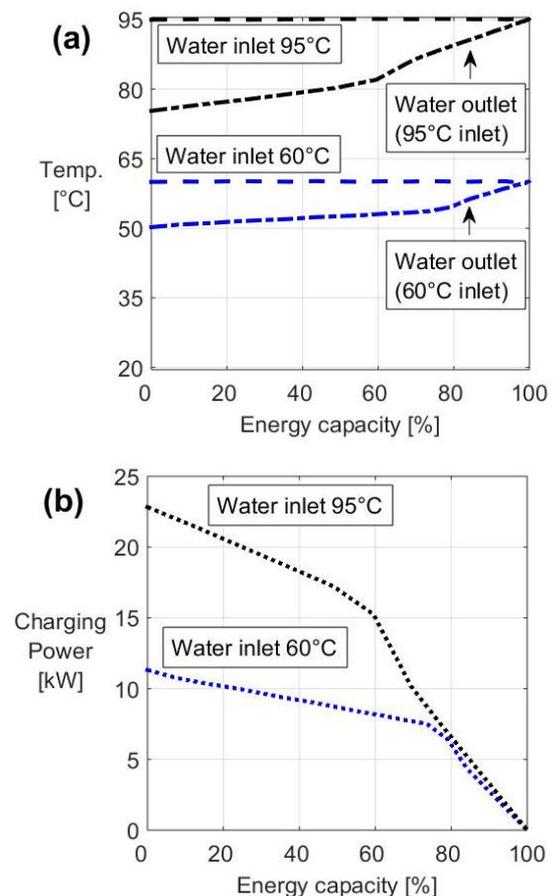

Figure 2: PCM ($CaCl_2 \cdot 6H_2O$) tank performance maps for charging from 0 % (21 °C) to 100 % (60 °C and 95 °C); (a) inlet and outlet water temperatures over energy capacity; (b) charging power over energy capacity.

BUILDING SIMULATION 2017

INTERNATIONAL
BUILDING
PERFORMANCE
SIMULATION
ASSOCIATION

Figure 3 shows the performance maps of the PCM tank using lauric acid as PCM. Lauric acid has a higher melting point (44 °C) and a lower heat conductivity than $CaCl_2 \cdot 6H_2O$ (Table 1). During charging, smaller temperature differences between supply and return water, lower charging power values, and an almost three times longer charging period (22 h compared to 8 h) are observed. The higher melting point also results in a steeper charging power decrease during 0 and 15 % of energy capacity (for 60 °C charging) and 0 and 10 % of energy capacity (for 95 °C charging) that is due to the sensible heat stored in the PCM (from 21 °C to 44 °C).
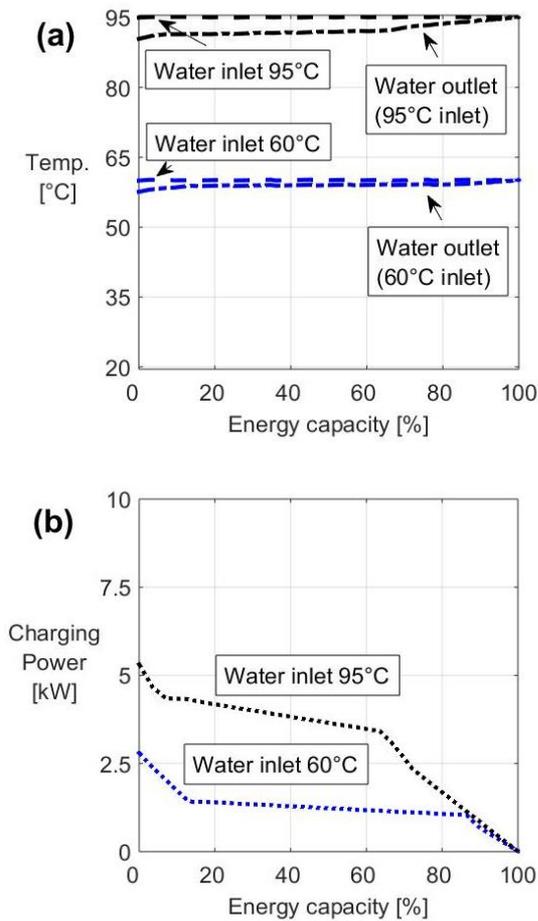

Figure 3: PCM (lauric acid) tank performance maps for charging from 0 % (21 °C) to 100 % (60 °C and 95 °C); (a) inlet and outlet water temperatures over energy capacity; (b) charging power over energy capacity.

Performance maps of TCM thermal energy storage

Figure 4 shows the performance maps of the TCM tank using zeolite13X-water as TCM. Charging the TCM starts at a temperature of 21 °C and a loading of 0.24 g/g (fully discharged). During the charging phase of 0 – 20 % of energy capacity, charging power is primarily applied to heat up the TCM to 95 °C or 120 °C. During the second phase between 20 % and 100 % of energy capacity, heat is used for desorption only. The entire charging process is completed after about 75 h.

Simulations are also conducted for silica gel–water as TCM. The charging temperatures are identical to the zeolite reactor with 95 °C or 120 °C. The initial conditions for silica gel-water are a temperature of 21 °C and a loading of 0.21 g/g. Due to a similar heat conductivity and diffusion coefficient, the heat and mass transfer dynamics of silica gel-water are similar to zeolite13X-water as shown in the performance maps in figure 4.
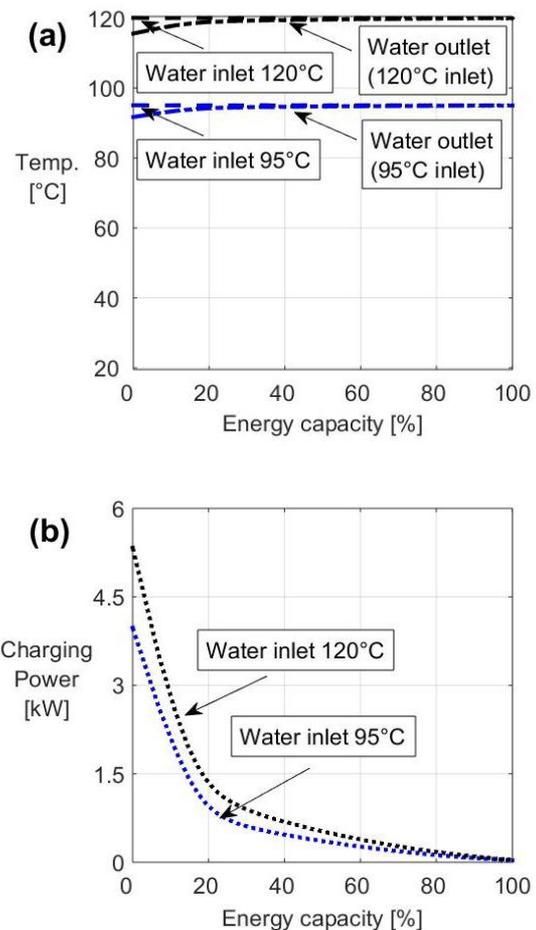

Figure 4: TCM (zeolite13X-water) tank performance maps for charging from 0 % (21 °C) to 100 % (95 °C and 120 °C); (a) inlet and outlet water temperatures over energy capacity; (b) charging power over energy capacity.

Thermal losses of TES tanks

The dynamic behavior of TES tanks considers the thermal losses during charging, discharging and idle mode. We use the introduced TES models to simulate typical values for the water tank, PCM tank, and TCM tank after 1 week in idle mode (Table 3). It is assumed that the TES tanks are placed in a constant environment of 21 °C.

BUILDING
SIMULATION 2017

INTERNATIONAL
BUILDING
PERFORMANCE
SIMULATION
ASSOCIATION

Table 3: Thermal losses of TES tanks after 1 week in idle mode (previously fully charged)

TES tank	Previously fully charged to [°C]	Thermal losses [%]
Water tank	60	42.2
	95	50.6
PCM tank	60	18.0
	95	27.5
TCM tank	95	7.5
	120	9.1

As can be seen from Table 3, the water tank shows the highest thermal losses because the main thermal resistance between heat storage medium and environment is the thermal insulation. The TCM tank has the lowest energy losses that relate only to the sensible heat stored in the TCM. There are no energy losses assumed for the chemical energy stored in the TCM.

Discussion

The knowledge of the dynamic behavior of TES is valuable information for predictive control (Masy et al., 2015; Patteeuw et al., 2015). The performance maps shown for the water tank, PCM tank, and TCM tank have all the operational parameters which represent the dynamic behavior during charging, discharging and idle mode. These operational parameters are listed below:

- Inlet and outlet water temperatures for charging and discharging
- State of charge
- Charging and discharging power
- Thermal losses

The operational parameters can be requested from the control for a specified time period, which can be a 15-minute time step or a 24 h prediction horizon. The performance maps can deliver the information based on the actual situation of the TES tank. To implement the performance maps in a predictive control, gray box or black box models can be applied. These models show an advantage over white box models concerning computational effort (Li and Wen, 2014).

The TES models used in this study are based on the one-dimensional convection-diffusion-reaction equation. They are solved numerically using the Crank-Nicolson scheme. Regarding computational speed, these models are well suited to be implemented in predictive control. However, these simplified models might affect the accuracy in predictive control. Especially for the PCM and TCM reactors, temperature, enthalpy and adsorbate distribution appears in the heat storage layer and not perpendicular to the storage layer. We propose the usage of the introduced finite-difference models as gray box models to represent the dynamic behavior of TES tank in predictive control. However, validations need to be done using measurement data.

Conclusion

We developed performance maps that represent all the operational parameters of TES tanks to be used in predictive control. These performance maps can be used in any situation during charging, discharging, and idle mode.

The dynamic behavior for the charging of water tanks, PCM tanks, and TCM tanks was simulated using the one-dimensional convection-diffusion-reaction equation. For each TES tank model, we developed a numerical solution based on the Crank-Nicolson scheme which is numerically stable and requires low computational effort. For the charging of water tanks, PCM tanks, and TCM tanks associated performance maps were presented. Based on these performance maps, we can conclude that stratified water tanks clearly outperform PCM tanks, and TCM tanks concerning potential charging power. This is due to heat convection in stratified water tanks as main heat transfer effect that results in high heat transfer values. The charging time varies between 44 min for the water tank, 8 – 22 h for the PCM tank and 75 h for the TCM tank. Thermal losses are the highest for water tanks and the lowest for TCM tanks. These parameters are crucial for determining demand flexibility. Water tanks are better suited to provide short-term flexibility, whereas PCM tanks and TCM tanks show an advantage in offering long-term flexibility.

Acknowledgement

References

Appadu, A.R., and Appadu, A.R. (2013). Numerical Solution of the 1D Advection-Diffusion Equation Using Standard and Nonstandard Finite Difference Schemes, Numerical Solution of the 1D Advection-Diffusion Equation Using Standard and Nonstandard Finite Difference Schemes. J. Appl. Math. J. Appl. Math. *2013*, *2013*, e734374.

De Coninck, R., and Helsen, L. (2016). Quantification of flexibility in buildings by cost curves – Methodology and application. Appl. Energy *162*, 653–665.

Deshmukh, H., Maiya, M.P., and Srinivasa Murthy, S. Study of sorption based energy storage system with silica gel for heating application. Appl. Therm. Eng.

Finck, C., Henquet, E., van Soest, C., Oversloot, H., de Jong, A.-J., Cuypers, R., and Spijker, H. van 't (2014). Experimental Results of a 3 kWh Thermochemical Heat Storage Module for Space Heating Application. Energy Procedia *48*, 320–326.

Finck, C.J., Spijker, J.C. van 't, Jong, A.J. de, Henquet, E.M.R., Oversloot, H.P., and Cuypers, R. Design of a modular 3 kWh thermochemical heat storage system for space heating application.

Hauer, A. (2007). Evaluation of adsorbent materials for heat pump and thermal energy storage applications in open systems. Adsorption 13, 399–405.

Hu, H., and Argyropoulos, S.A. (1996). Mathematical modelling of solidification and melting: a review. Model. Simul. Mater. Sci. Eng. 4, 371.

de Jong, A.-J., Trausel, F., Finck, C., van Vliet, L., and Cuypers, R. (2014). Thermochemical Heat Storage – System Design Issues. Energy Procedia 48, 309–319.

Karahan, H. (2006). Implicit finite difference techniques for the advection–diffusion equation using spreadsheets. Adv. Eng. Softw. 37, 601–608.

Lamberg, P. (2003). Mathematical modelling and experimental investigation of melting and solidification in a finned phase change material storage. Helsinki University of Technology.

Leong, K.C., and Liu, Y. (2006). System performance of a combined heat and mass recovery adsorption cooling cycle: A parametric study. Int. J. Heat Mass Transf. 49, 2703–2711.

Li, X., and Wen, J. (2014). Review of building energy modeling for control and operation. Renew. Sustain. Energy Rev. 37, 517–537.

Lim, K., Che, J., and Lee, J. (2017). Experimental study on adsorption characteristics of a water and silica-gel based thermal energy storage (TES) system. Appl. Therm. Eng. 110, 80–88.

Lo Brano, V., Ciulla, G., Piacentino, A., and Cardona, F. (2014). Finite difference thermal model of a latent heat storage system coupled with a photovoltaic device: Description and experimental validation. Renew. Energy 68, 181–193.

Masy, G., Georges, E., Verhelst, C., Lemort, V., and André, P. (2015). Smart grid energy flexible buildings through the use of heat pumps and building thermal mass as energy storage in the Belgian context. Sci. Technol. Built Environ. 21, 800–811.

Mosaffa, A.H., Garousi Farshi, L., Infante Ferreira, C.A., and Rosen, M.A. (2014). Energy and exergy evaluation of a multiple-PCM thermal storage unit for free cooling applications. Renew. Energy 68, 452–458.

Oldewurtel, F., Sturzenegger, D., Andersson, G., Morari, M., and Smith, R.S. (2013). Towards a standardized building assessment for demand response. (IEEE), pp. 7083–7088.

Ottesen, S.O., and Tomasgard, A. (2015). A stochastic model for scheduling energy flexibility in buildings. Energy 88, 364–376.

Patteeuw, D., Bruninx, K., Arteconi, A., Delarue, E., D'haeseleer, W., and Helsen, L. (2015). Integrated modeling of active demand response with electric heating systems coupled to thermal energy storage systems. Appl. Energy 151, 306–319.

Pereira da Cunha, J., and Eames, P. (2016). Thermal energy storage for low and medium temperature applications using phase change materials – A review. Appl. Energy 177, 227–238.

Pesaran, A., Lee, H., Hwang, Y., Radermacher, R., and Chun, H.-H. (2016). Review article: Numerical simulation of adsorption heat pumps. Energy 100, 310–320.

Recktenwald, G.W. (2000). Numerical Methods with MATLAB: Implementations and Applications (Prentice Hall).

Rindt, C.C.M., and Gaastra-Nedea, S.V. (2015). 15 - Modeling thermochemical reactions in thermal energy storage systems. In Advances in Thermal Energy Storage Systems, L.F. Cabeza, ed. (Woodhead Publishing), pp. 375–415.

Sayılgan, Ş.Ç., Mobedi, M., and Ülkü, S. (2016). Effect of regeneration temperature on adsorption equilibria and mass diffusivity of zeolite 13x-water pair. Microporous Mesoporous Mater. 224, 9–16.

Shukla, A., Singh, A.K., Singh, P., Shukla, A., Singh, A.K., and Singh, P. (2011). A Comparative Study of Finite Volume Method and Finite Difference Method for Convection-Diffusion Problem. Am. J. Comput. Appl. Math. 1, 67–73.

Tatsidjodoung, P., Le Pierrès, N., Heintz, J., Lagre, D., Luo, L., and Durier, F. (2016). Experimental and numerical investigations of a zeolite 13X/water reactor for solar heat storage in buildings. Energy Convers. Manag. 108, 488–500.

Wang, Y., and LeVan, M.D. (2009). Adsorption Equilibrium of Carbon Dioxide and Water Vapor on Zeolites 5A and 13X and Silica Gel: Pure Components. ResearchGate 54.